An Effective Method of Magnetic Hyperthermia Based on the Ferromagnetic Resonance Phenomenon

S. V. Stolyar[a, b,]*, **O. A. Li**[a, b], **E. D. Nikolaeva**[a], **A. M. Vorotynov**[c], **D. A. Velikanov**[c], **Yu. V. Knyazev**[c],
O. A. Bayukov[c], **R. S. Iskhakov**[c], **V. F. P'yankov**[a], and **M. N. Volochaev**[c]

[a] *Federal Research Center, Siberian Branch, Russian Academy of Sciences, Krasnoyarsk, 660036 Russia*
[b] *Siberian Federal University, Krasnoyarsk, 660041 Russia*
[c] *Institute of Physics, Siberian Branch, Russian Academy of Sciences, Krasnoyarsk, 660036 Russia*
*e-mail: stol@iph.krasn.ru

Abstract—Nickel and cobalt ferrite nanoparticles have been synthesized using the chemical precipitation method; the nanoparticle sizes were found to be 63 ± 22 and 26 ± 4 nm, respectively. The static hysteresis loops and Mössbauer spectra have been measured. It is shown that cobalt ferrite powders are magnetically harder than nickel ferrite powders. Ferromagnetic resonance (FMR) curves have been studied. It is found that the FMR absorption for cobalt ferrite is observed at room temperature and above. The time dependences of the nanoparticle warm-up under FMR conditions have been measured. The maximum temperature changes for nickel ferrite and cobalt ferrite particles are 8 and 11 K, respectively. Using the example of cobalt ferrite powder, the possibility of effectively heating of particles in the FMR mode in their own field without using a DC magnetic field source is shown. The observed effect can be used in magnetic hyperthermia.

INTRODUCTION

Hyperthermia is considered one of the auxiliary methods of treatment of oncological diseases through a general or local increase of the temperature up to 41–46°C. This effect is associated with the fact that tumor cells are more sensitive to sudden temperature rises compared to healthy cells and with the peculiarities of the microstructure of tumors, namely, an acidic medium and hypoxia. In vivo, hyperthermia increases blood flow and oxygenation inside tumors and promotes the delivery of drugs and remedies, thereby enhancing the effects of chemo- and radiotherapy [1].

For magnetic hyperthermia based on heat release during magnetization reversal of a magnetic material, magnetic nanoparticles composed of metals or iron oxides and magnetic ferrites doped with Mn, Co, Ni, or Zn are used. The advantages of using ferromagnetic (ferrimagnetic) nanoparticles are the low cost of their production, their chemical stability, biocompatibility, and the possibility of surface modification.

For practical therapeutic applications with minimal side effects, it is very important to obtain optimal heating efficiency to achieve a desired hyperthermia temperature of 41–46°C, since thermal ablation occurs at temperatures above 50°C [2]. To protect healthy tissues from overheating, it is necessary to limit the applied field both in amplitude and in frequency, that is, the maximum permissible field intensity (Brezovich limit) when exposing the whole body is $fH = 4.85 \times 10^8$ A/(m s) [3]. This limit can be exceeded under local exposure, in particular, the characteristic values of $fH \approx (10^{10}-10^{11})$ A/(m s) are used in magnetic resonance imaging [4]. For magnetic hyperthermia, frequencies f of around 100 kHz and magnetic fields H of around 100 Oe (1 Oe = 80 A/m) are used [5].

At present, studies of magnetic nanoparticles for hyperthermia based on magnetization reversal processes are focused on determining the optimal dose of nanoparticles and the magnetization reversal parameters [6].

Magnetic nanoparticles can be heated using the phenomenon of ferromagnetic resonance (FMR) associated with the resonance absorption of the energy of a ultra-high-frequency (UHF) electromagnetic field when the ultra high frequency and the precession frequency of magnetization vector **M** around the direction of applied external magnetic field H coincide. In this case, the specific power absorbed by the ferromagnet is determined by expression $P = \omega \chi H^2$, where ω is the ultra high frequency, χ is the imaginary component of the magnetic susceptibility under resonance conditions, and H is the amplitude of the magnetic component of the UHF field [7]. The idea of
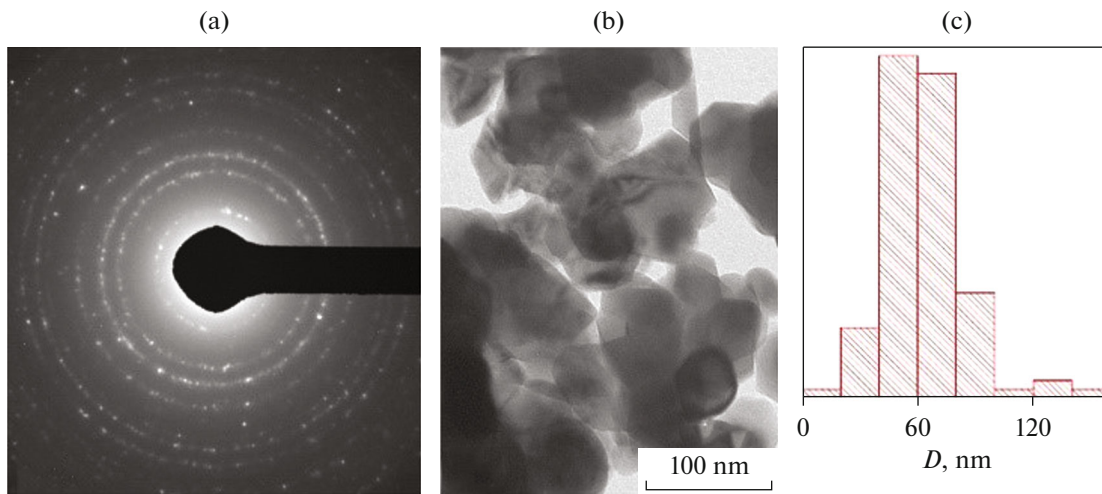
Fig. 1. (a) The electron diffraction pattern and (b) microphotograph of nickel ferrite particles after annealing; (c) particle size distribution.

using the FMR technique in magnetic hyperthermia applications was expressed in [4, 8, 9].

This study is devoted to testing the possibility of heating ferrite nanoparticles obtained by chemical precipitation. The aim of the study was to investigate the peculiarities of nanoparticle heating under FMR conditions using soft (nickel ferrite) and hard (cobalt ferrite) magnetic powders as examples. For testing the manufactured ferrites, both structural (electron microscopy) and magnetic (measurement of static magnetization reversal curves) and Mössbauer spectroscopy) methods were used.

EXPERIMENTAL

Magnetic nanoparticles doped with nickel and cobalt were synthesized by chemical coprecipitation, as follows: 0.2 mol of $NiSO_4 \cdot 7H_2O$ or $CoSO_4 \cdot 7H_2O$ and 0.4 mol of $FeCl_3 \cdot 6H_2O$ were dissolved in 100 mL of distilled water, and then NH_4OH was added dropwise until reaching pH 11 and heated under constant stirring to 80°C for 30 min. The resulting precipitate was then washed, collected, and annealed at 700°C for 5 h. The resulting material was ground in a mortar.

The microphotographs were made using a Hitachi HT7700 transmission electron microscope. The magnetic properties were measured using a vibration-sample magnetometer.

The ferromagnetic resonance (FMR) spectra were recorded at a frequency of 8.9 GHz on a SE/X-2544 spectrometer at the Krasnoyarsk Regional Center for Collective Use, Federal Research Center Krasnoyarsk Scientific Center, Siberian Branch, Russian Academy of Sciences.

The Mössbauer spectra of the studied samples were recorded on an MS-1104Em spectrometer in the transmission geometry mode with a $Co^{57}(Rh)$ radio-

active source at a temperature of 300 K. The modulating signal of the motion of the radioactive source was set by a triangular pulse. A sample with a relative thickness of 5 mg/cm^2 was placed on aluminum foil with a thickness of 10 μm.

RESULTS AND DISCUSSION

Transmission electron microscopy images of ferrite particles and size distributions of particles are shown in Figs. 1 and 2. Particles have different shapes, such as cubes, sticks, scales, and polyhedral formations. For particles with complex shapes, the average size between the maximum and minimum sizes was taken as a characteristic size. The average particle sizes for nickel ferrite and cobalt ferrite were 63 ± 22 and 26 ± 4 nm, respectively.

The hysteresis loops of nickel and cobalt ferrite particles are shown in Figs. 3 and 4, respectively. The hysteresis loops of nickel ferrite particles slightly change with an increase in the temperature and coercive force H_c decreases from 210 to 140 Oe when heated from 80 to 295 K. The hysteresis loops of cobalt ferrite particles at low temperatures are partial in these fields, since the coercive force at 80 K exceeds 10 kOe. The limiting loop was obtained only at room temperature and the coercive force was 720 Oe.

In high fields (the magnetization approaches saturation magnetization), the dependence of the magnetization on the field strength follows Akulov's law [10−13] given by formula

$$M(H) = M_S \left(1 - \left(aH_a/H\right)\right)^2, \qquad (1)$$

where M_s is the saturation magnetization; $H_a = 2K/M_s$ is the local magnetic anisotropy field; K is the energy of local magnetic anisotropy of particles; and a is the coefficient determined by the symmetry of magnetic
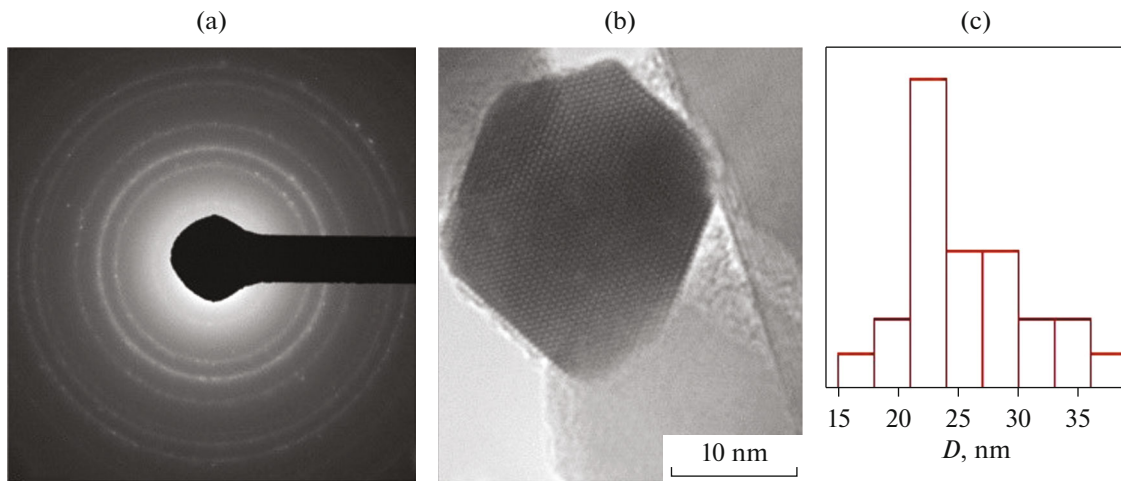
Fig. 2. (a) The electron diffraction pattern and (b) microphotograph of cobalt ferrite particles after annealing; (c) particle size distribution.

anisotropy, which is equal to $(2/105)^{1/2}$ for cubic magnetic anisotropy and $(1/15)^{1/2}$ for uniaxial anisotropy.

The approximation of measured dependences $M(H)$ by equation (1) allowed us to find the saturation magnetization M_s and the root-mean-square fluctuation of the local magnetic anisotropy field aH_a, as well as to determine the value of the local magnetic anisotropy H_a. The calculation results are given in Table 1.

The Mössbauer spectra of the studied samples are shown in Figs. 5 and 6. Tables 2 and 3 show the results of interpreting the spectra. The spectra in both cases are sextets (Figs. 5a and 6a) that correspond to the inverted spinel structure. Possible nonequivalent positions of iron in the samples were determined from the calculation of the probability distribution of quadrupole splittings and hyperfine fields in the experimental spectra. In accordance with the obtained results, a preliminary model spectrum of the sample was simu-

lated. The model spectra were fitted to the experimental spectra by varying the entire set of hyperfine parameters with use of the least-squares method in the linear approximation.

For each sample, two P(QS) distributions were obtained, one for a relatively large chemical shift (IS = 0.35−0.40 mm/s, blue squares) and the other for a small chemical shift (IS = 0.22−0.28 mm/s, red circles). According to the chemical shifts (IS), we can say that iron is in the 3^+ charge state in both samples. Moreover, different local environments are characterized by different electron densities. Considering that the spinel structure has two types of positions, such as tetrahedral positions A and octahedral positions B, it is possible to obtain the distribution of iron over these positions in the samples (the last column in Tables 2 and 3). The Mössbauer parameters of quadrupole doublets with smaller chemical shifts are characteristic
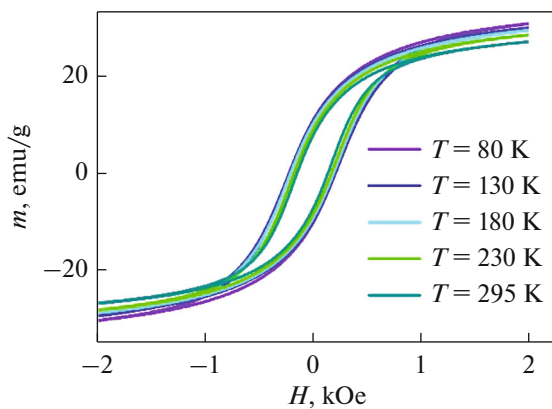
Fig. 3. The dependences of the magnetization of nickel ferrite on the magnetic field strength at different temperatures.
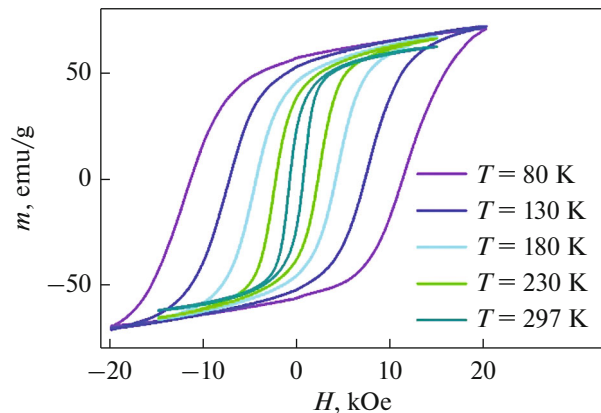
Fig. 4. The dependences of magnetization M of cobalt ferrite on the magnetic field strength at different temperatures.

Table 1. The hysteresis loop parameters at room temperature

Sample	H_c, Oe	M_s, emu/g	aH_a, kOe	H_a, kOe	
				$a = (2/105)^{1/2}$	$a = (1/15)^{1/2}$
$NiFe_2O_4$	141	34	2.32	16.8	9.0
$CoFe_2O_4$	720	64	2.83	20.6	11

Table 2. The Mössbauer parameters of nickel ferrite

IS, ±0.005 mm/s	H_{hf}, ±2 kOe	QS, ±0.02 mm/s	W, ±0.02 mm/s	A, ±0.03	Position
0.37	524	−0.01	0.26−0.46	0.39	Fe^{3+}(B)
0.38	518	−0.46	0.27	0.14	Fe^{3+}(B)
0.26	490	0	0.48	0.47	Fe^{3+}(A)

IS is the isomeric chemical shift with respect to α-Fe, H_{hf} is the hyperfine field, QS is the quadrupole splitting, W is the linewidth, and A is the fractional occupancy of the site.

Table 3. The Mössbauer parameters of cobalt ferrite

IS, ±0.005 mm/s	H_{hf}, ±2 kOe	QS, ±0.02 mm/s	W, ±0.02 mm/s	A, ±0.03	Position
0.40	505	0.12	0.29−0.50	0.12	Fe^{3+}(B)
0.37	474	0.02	0.52	0.20	Fe^{3+}(B)
0.36	450	0	0.44−0.79	0.16	Fe^{3+}(B)
0.35	420	−0.12	0.62−1.63	0.20	Fe^{3+}(B)
0.28	485	0	0.43	0.18	Fe^{3+}(A)
0.22	472	−0.10	0.27−0.52	0.14	Fe^{3+}(A)

IS is the isomeric chemical shift with respect to α-Fe, H_{hf} is the hyperfine field, QS is the quadrupole splitting, W is the linewidth, and A is the fractional occupancy of the site.

of the high-spin Fe^{3+} cation in oxides [14], for which positions with IS < 0.3 mm/s refer to tetrahedral oxygen coordination, and positions with IS > 0.3 mm/s refer to octahedral coordination by oxygen. Figures 5b and 6b show the probability distributions of hyperfine fields on iron nuclei in tetrahedral and octahedral positions. Additional positions in the B sublattice of nickel ferrite occur because of the disordered distribution of iron and nickel in this sublattice. The octahedral
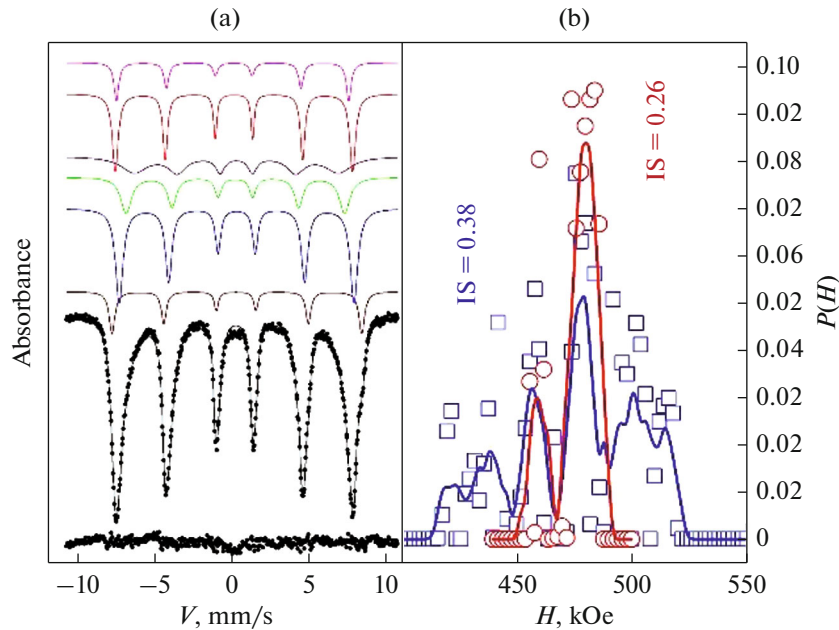
positions in the spectrum of cobalt ferrite are represented by four sextets. The multiplicity of sextets indicates a chaotic distribution of cobalt and iron over spinel positions. The measured occupancies of nonequivalent iron positions lead approximately to the following ferrite formulas: $(Co_{0.36}Fe_{0.64})[Co_{0.64}Fe_{1.36}]O_4$ and $(Fe)[Ni_{0.94}Fe_{1.06}]O_4$.

The observed wide distribution of the probability of hyperfine fields on iron nuclei in octahedral positions in cobalt ferrite agrees with the obtained chemical formula of the crystal. It implies a high concentration inhomogeneity of the distribution of cobalt and iron cations in the sample. This is associated with the fact that cobalt cations in the spinel structure can occupy both tetrahedral and octahedral positions. At the same
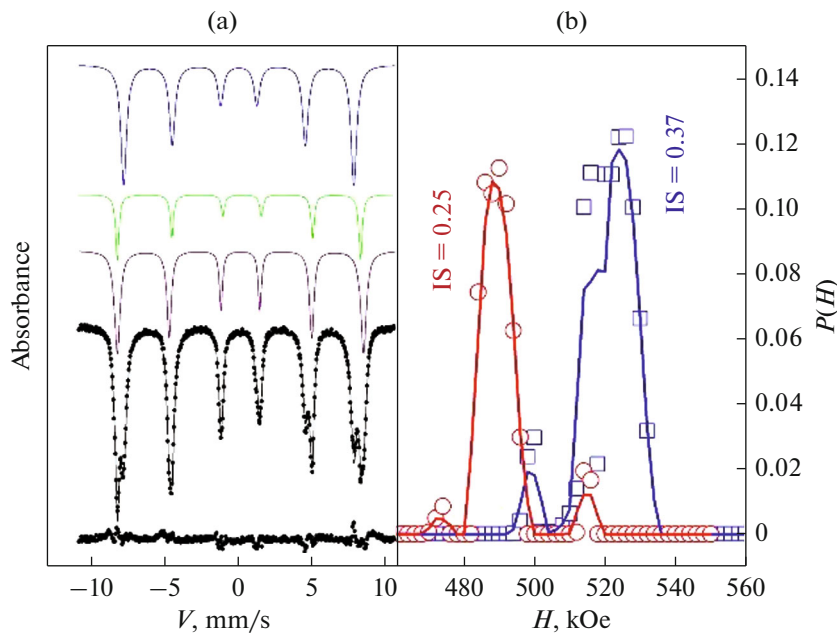
Fig. 5. (a) The room temperature Mössbauer spectrum of nickel ferrite; the lower plot is the difference spectrum. (b) The probability distribution of hyperfine fields over iron nuclei in tetrahedral (red line) and octahedral (blue line) positions.

Fig. 6. (a) The room temperature Mössbauer spectrum of cobalt ferrite; the lower plot is the difference spectrum. (b) The probability distribution of hyperfine fields over iron nuclei in tetrahedral (red line) and octahedral (blue line) positions.
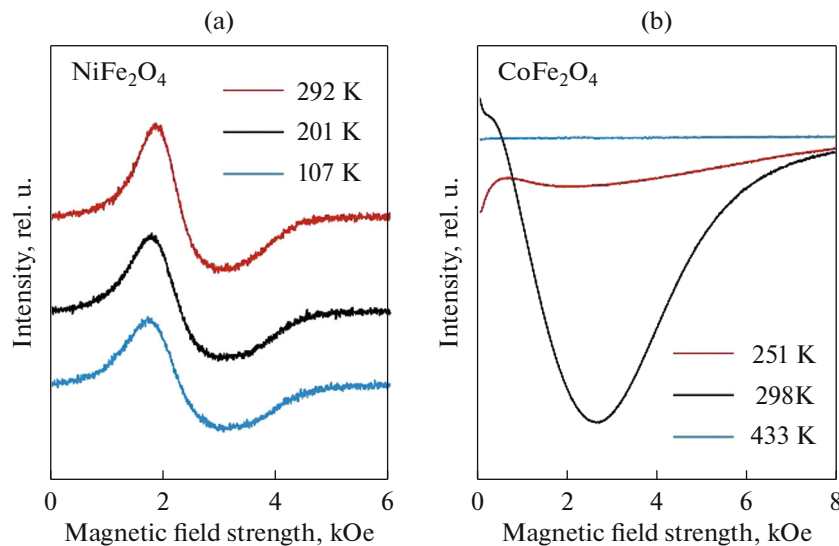

Fig. 7. The ferromagnetic resonance spectra of (a) nickel ferrite and (b) cobalt ferrite at different temperatures.

time, nickel cations in Ni ferrite tend to occupy only octahedral positions [15]. It is possible that the concentration inhomogeneity of the distribution of cobalt and iron cations in cobalt ferrite powders is the reason for the high values of coercive fields H_c in cobalt ferrite ($H_c = 10$ kOe at $T = 80$ K, and $H_c = 720$ Oe at $T = 297$ K).

The differential lines of the ferromagnetic resonance recorded at different temperatures are shown in Fig.7. The resonance field for nickel ferrite slightly increases with an increase in the temperature (Fig. 7a). The ferromagnetic resonance linewidth ΔH at room temperature is $\Delta H \approx 1$ kOe. The measurement results for cobalt ferrite (Fig. 7b) indicate that the absorption of UHF energy of powders in the FMR mode is absent almost up to room temperatures, which is associated with the magnetic hardness of this ferrite and correlates with hysteresis loops that have high values of the coercive force and the anisotropy field. The full width at half maximum of the resonance
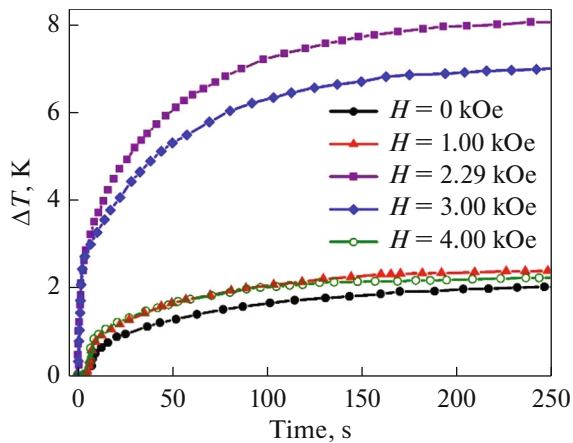
Fig. 8. The time dependences of the temperature increment of nickel ferrite particles under different magnetic field strengths.
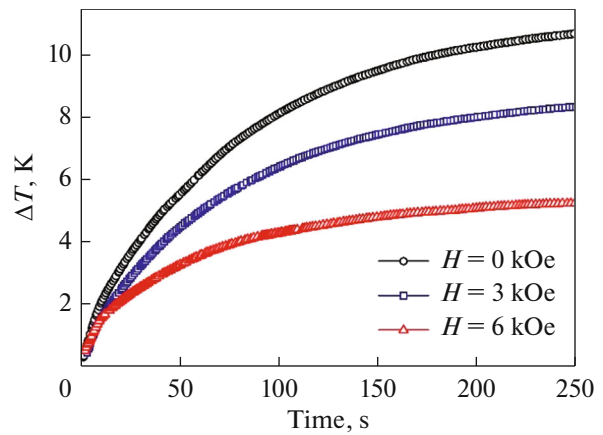
Fig. 9. The time dependences of the temperature increment of cobalt ferrite particles under different magnetic field strengths.

absorption line at $T = 344$ K (at this temperature, half of the FMR curve have been formed) is $\Delta H/2 \approx 3$ kOe.

In our opinion, the high values of the FMR linewidth (as well as the high values of the coercive field) for cobalt ferrite are determined by the concentration inhomogeneity of the distribution of cobalt and iron cations. Thus, the width of hyperfine field distribution at iron nuclei over octahedral sites in cobalt ferrite is more than 100 kOe, according to Fig. 6b.

The absence of resonance absorption indicates the presence of a gap in frequency–field dependence $f(H)$ of cobalt ferrite powders, which depends on temperature. The appearance of FMR at room temperature makes it possible to estimate the magnitude of this gap. The frequency of the UHF field used in our study is 8.9 GHz, and the gyromagnetic ratio is $\gamma = 2.9$ GHz/kOe. Therefore, the gap expressed in the field is $H_0 = f/\gamma \approx 3$ kOe at room temperature.

For practical applications, it is necessary to heat the particles in a narrow temperature range. The temperature increment depends on the absorbed power and exposure duration. We have studied the time dependence of temperature change ΔT of particles in an alternative current (AC) magnetic field with a frequency of 8.9 GHz and an amplitude of about 1 Oe for various values of a direct current (DC) magnetic field applied perpendicular to the AC one. The temperature of nanoparticles was measured using a T-type thermocouple, in which the material of the positive electrode was copper (Cu) and the material of the negative electrode was constantan alloy (55 wt % Cu + 45 wt % Ni, Mn, and Fe). Figures 8 and 9 show the results of these studies. In all cases, we observe a sharp increase in the temperature at the initial point in time, which is followed by a decrease in the temperature increment upon reaching saturation condition ΔT_{max}. For nickel ferrite, the warm-up of particles increases to the maximum value $\Delta T_{max} = 8.2$ K with an increase in the

strength of the applied DC field to a strength of $H = 2.29$ kOe; with a further increase in the strength, the warm-up of the particles decreases. The obtained value of the warm-up agrees with the published data [9]. The maximum temperature increment in a field of 2.29 kOe can be explained by the fact that the resonance absorption of the electromagnetic field at a frequency of 8.9 GHz is observed with this field strength, as can be seen from the results of measuring the ferromagnetic resonance spectra (Fig. 7a).

For more magnetically hard cobalt ferrite, the highest warm-up, $\Delta T_{max} = 10$ K, was obtained in the absence of a DC magnetic field ($H = 0$), and the temperature change decreases with an increase in the strength of the DC magnetic field. The largest increase in the temperature in the absence of an external field can be explained by resonance UHF absorption in the internal field of nanoparticles, which is $H_0 = f/\gamma \approx 3$ kOe at room temperature, or natural ferromagnetic resonance. In our opinion, this experimental result is important for practical applications of magnetic hyperthermia, since it demonstrates the possibility of heating magnetic nanoparticles in the FMR mode in the absence of an external magnetic field.

CONCLUSIONS

Particles of nickel ferrite $NiFe_2O_4$ with a size of 63 nm and particles of cobalt ferrite $CoFe_2O_4$ with a size of 26 nm were synthesized by chemical precipitation.

The static hysteresis loops of the synthesized powders were measured. It has been shown that cobalt ferrite powders are magnetically harder substances.

Using Mössbauer spectroscopy, the occupancies of nonequivalent iron sites have been determined and the following formulas of ferrites, which indicate a high concentration inhomogeneity of the distribution of

cobalt and iron in cobalt ferrite, have been obtained: $(Co_{0.36}Fe_{0.64})[Co_{0.64}Fe_{1.36}]O_4$ and $(Fe)[Ni_{0.94}Fe_{1.06}]O_4$.

The ferromagnetic resonance curves and the time dependences of the temperature of particles upon absorption of the energy of a UHF field at a frequency of 8.9 GHz have been studied. It has been determined that the highest warm-up of nickel ferrite particles is observed under a DC magnetic field strength equal to resonance field $H = 2.29$ kOe. The greatest warm-up of cobalt ferrite particles in the absence of an applied DC magnetic field is caused by natural ferromagnetic resonance in the internal field of the particles. The observed effect can be used in the practice of magnetic hyperthermia in a new method of heating particles in the ferromagnetic resonance mode: the heating can be conducted quite efficiently in a particle's own field without using a DC magnetic field source.

CONFLICT OF INTEREST

The authors declare that they have no conflicts of interest.

REFERENCES

1. M. Peiravi, H. Eslami, M. Ansari, and H. Zare-Zardini, "Magnetic hyperthermia: Potentials and limitations," J. Indian Chem. Soc. **99**, 100269 (2022).
https://doi.org/10.1016/j.jics.2021.100269

2. D. Ho, X. Sun, and Sh. Sun, "Monodisperse magnetic nanoparticles for theranostic applications," Acc. Chem. Res. **44**, 875–882 (2011).
https://doi.org/10.1021/ar200090c

3. I. A. Brezovich, W. J. Atkinson, and M. B. Lilly, "Local hyperthermia with interstitial techniques," Cancer Res. **44**, 4752s–4756s (1984).

4. J.-H. Lee, B. Kim, Y. Kim, and S.-K. Kim, "Ultrahigh rate of temperature increment from superparamagnetic nanoparticles for highly efficient hyperthermia," Sci. Rep. **11**, 4969 (2021).
https://doi.org/10.1038/s41598-021-84424-1

5. A. S. Kamzin, D. S. Nikam, and S. H. Pawar, "Study of Co/0.5Zn0.5Fe$_2$O$_4$ nanoparticles for magnetic hyperthermia," Phys. Solid State **59**, 156–163 (2017).
https://doi.org/10.1134/S1063783417010127

6. X. Liu, Y. Zhang, Y. Wang, W. Zhu, G. Li, X. Ma, Y. Zhang, S. Chen, S. Tiwari, K. Shi, S. Zhang, H. M. Fan, Y. X. Zhao, X.-J. Liang, "Comprehensive understanding of magnetic hyperthermia for improving antitumor therapeutic efficacy," Theranostics **10**, 3793–3815 (2020).
https://doi.org/10.7150/thno.40805

7. *Ferromagnetic resonance: Phenomenon of Resonance Absorption of the High-Frequency Electromagnetic Field in Ferromagnetic Substances*, Ed. by S. V. Vonsovskii (Fizmatlit, Moscow, 1961).

8. I. Khmelinskii and V. I. Makarov, "EPR hyperthermia of *S. cerevisiae* using superparamagnetic Fe$_3$O$_4$ nanoparticles," J. Therm. Biol. **77**, 55–61 (2018).
https://doi.org/10.1016/j.jtherbio.2018.08.004

9. J.-H. Lee, Y. Kim, and S.-K. Kim, "Highly efficient heat-dissipation power driven by ferromagnetic resonance in MFe$_2$O$_4$ (M = Fe, Mn, Ni) ferrite nanoparticles," Sci. Rep. **12**, 5232 (2022).
https://doi.org/10.1038/s41598-022-09159-z

10. N. S. Akulov, *Ferromagnetism* (Gos. Izd-vo Tekhniko-Teoreticheskoi Literatury, Moscow, 1939).

11. N. S. Akulov, "Über den Verlauf der Magnetisierungskurve in starken Feldern," Z. Phys. **69**, 822–831 (1931).
https://doi.org/10.1007/BF01339465

12. V. A. Ignatchenko and R. S. Iskhakov, "Stochastic magnetic structure and spin waves in amorphous ferromagnetic substance," Izv. Akad. Nauk SSSR. Ser. Fiz. **44**, 1434–1437 (1980).

13. L. A. Chekanova, E. A. Denisova, O. A. Goncharova, S. V. Komogortsev, and R. S. Iskhakov, "Analysis of phase composition of Co–P alloy powders using magnetometric data," Phys. Met. Metallogr. **114**, 122–128 (2013).
https://doi.org/10.1134/S0031918X1302004X

14. F. Menil, "Systematic trends of the ^{57}Fe Mössbauer isomer shifts in (FeO$_n$) and (FeF$_n$) polyhedra. Evidence of a new correlation between the isomer shift and the inductive effect of the competing bond T–X ($\rightarrow$ Fe) (where X is O or F and T any element with a formal positive charge)," J. Phys. Chem. Solids **46**, 763–789 (1985).

15. Krupička, S., *Physik der Ferrite und der verwandten magnetischen Oxide* (Academia, Prague, 1973).
https://doi.org/10.1007/978-3-322-83522-2

Translated by O. Kadkin